Journal of Materials Chemistry A

Accepted Manuscript

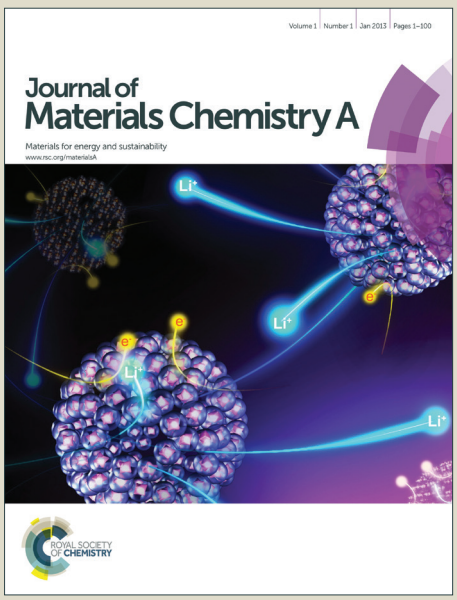

ROYAL SOCIETY OF CHEMISTRY

www.rsc.org/materialsA

Cite this: DOI: 10.1039/c0xx00000x

www.rsc.org/xxxxxx

ARTICLE TYPE

Cobalt sulfide nanosheets coated on $NiCo_2S_4$ nanotube arrays as electrode materials for high-performance supercapacitors

Wenbin Fu, Changhui Zhao,Weihua Han,* Ying Liu, Hao Zhao, Yufang Ma and Erqing Xie*

Received (in XXX, XXX) XthXXXXXXXXX 20XX, Accepted Xth XXXXXXXXX 20XX

DOI: 10.1039/b000000x

Hierarchical hybrid electrodes were successfully fabricated by electrodeposition of ultrathin cobalt sulfide (CoS_x) nanosheets on $NiCo_2S_4$ nanotube arrays grown on Ni foam for high-performance supercapacitors. The hierarchical $NiCo_2S_4$@CoS_x core/shell nanotube arrays exhibit a high areal capacitance (4.74 F cm^{-2} at a current density of 5 mA cm^{-2}), a good rate capability (2.26 F cm^{-2} at 50 mA cm^{-2}) and cycle stability (76.1% capacitance retention after 1500 cycles at a high current density of 50 mA cm^{-2}), which are much better than those of the $NiCo_2S_4$ nanotubes. Such superior electrochemical performance could be attributed to the smart configuration of the two electroactive materials. It can provide more pathways for electron transport and improve the utilization rate of electrode materials. This effective strategy shows the feasibility of designing and fabricating metal sulfides with core/shell hybrid structures as electrode materials for high-performance supercapacitors.

1. Introduction

The intermittency and unportable problems of current electric generators, such as photovoltaics and wind turbines, have made energy storage one of the great challenges in 21 century.[1] Among various energy storage devices, supercapacitors, which can store the intermittency energy in a portable manner and make the energy accessible upon demand, are highly considered as a promising candidate due to their high power density, fast charge-discharge process and long cycle life.[2-4] Based on the energy storage mechanism, supercapacitors can be divided into two categories: electrical double-layer capacitors (EDLCs) and pseudocapacitors. In EDLCs, electrical energy is stored by electrostatic accumulation of charges in the electric double-layer at the electrode/electrolyte interfaces, such as carbon materials. While pseudocapacitors, making use of the surface fast reversible redox reactions, can possess much higher specific capacitance and energy density than EDLCs.[5-7] Transition metal oxides and hydroxides were widely investigated as electrode materials for pseudocapacitors because of their high theoretical specific capacitance, environmental friendliness and low cost.[8-12] However, the poor conductivity of most transition metal oxides and hydroxides impede the electron transport, resulting in the gradual loss of capacitance and hindering their practical applications in supercapacitors.[13, 14] Therefore, it is expected to design and fabricate electrode materials with high capacitive performance as well as good electrical conductivity.

Recently, transition metal sulfides (such as CoS,[15] CoS_2,[16] Ni_3S_2,[17] CuS,[18] etc.) have been utilized as electrode materials which have high electrical conductivity, good mechanical and thermal stability and excellent electrochemical performance in supercapacitors.[19, 20] As electrode materials, cobalt sulfides (CoS, CoS_2, Co_3S_4, Co_9S_8, etc.) have attracted great attention in light of their high capacitance, good rate capability and excellent cycling stability.[21, 22] Among transition metal sulfides, binary $NiCo_2S_4$ exhibits much higher electric conductivity in comparison with $NiCo_2O_4$, CoS and Ni_3S_2. With both nickel and cobalt ions, $NiCo_2S_4$ can offer richer redox reactions than the corresponding single component sulfides (Ni_3S_2 or Co_9S_8).[23-25] Practically, $NiCo_2S_4$ nanotube arrays grown on conductive substrates can have large surface areas, good mechanical adhesion and electrical contact with the substrate. More attractively, they can exhibit high capacitive performance and such merits make them very promising for applications in supercapacitors.[26, 27]

Previous work revealed that the diffusion distance of the electrolyte into the electrode materials is extremely short (~20 nm). It is difficult for all the active materials to participate in the electrochemical charge storage processes and only the near surface part can effectively contribute to the total capacitance of the electrode.[28, 29] To improve the electrochemical utilization of the active materials, pseudocapacitive materials with various configurations have been designed and built for supercapacitors. Particularly, the core/shell hybrid structures with the combination of two materials or structures on conductive substrates have been considered as binder-free electrodes for supercapacitors with favorable capacitive performance.[30-32] The core structures directly grown on the conductive substrate create a tight physical contact with the substrate as the electron transport path. The shells on the cores could dramatically increase the interface between the electrode and the electrolyte.[33, 34] In view of the predictable advantages, various configurations of core/shell hybrid structures, such as Co_3O_4@$NiCo_2O_4$,[32] ZnO@Ni_3S_2,[17] $NiCo_2O_4$@MnO_2[35] and $ZnCo_2O_4$@$Ni(OH)_2$,[36] have been designed and investigated for high-performance supercapacitors. However, there is little

literature on the core/shell hybrid structures with the combination of two metal sulfides materials for supercapacitors.

In this work, hierarchical $NiCo_2S_4$@CoS_x core/shell nanotube arrays (NTAs) grown on Ni foam were successfully fabricated by an effective strategy. The $NiCo_2S_4$ nanotubes with a thin wall have a diameter of 60–100 nm and a length of 2–4 μm. The ultrathin CoS_x nanosheets with silk-like morphology coated on the $NiCo_2S_4$ nanotubes and connected some of them together. This hierarchical hybrid structures can make efficient use of the advantages of the two electroactive materials, such as high electrical conductivity, rich redox reactions and tiny structures. Electrochemical measurements show that the hierarchical $NiCo_2S_4$@CoS_x core/shell NTAs have superior electrochemical performance with high areal capacitance, good rate capability and cycle stability.

2. Experimental

2.1 Synthesis of $NiCo_2S_4$ NTAs on Ni foam

All the reagents used were of analytical grade and used without further purification. The $NiCo_2S_4$ NTAs were synthesized by a hydrothermal method followed by an anion exchange reaction. Prior to the synthesis, a piece of Ni foam was carefully cleaned with 3 M HCl solution in an ultrasonic bath for 10 min to remove the oxide layer, then rinsed with deionized water and ethanol, sequentially. 2 mmol $NiCl_2{\cdot}6H_2O$, 4 mmol $CoCl_2{\cdot}6H_2O$ and 12 mmol urea were dissolved in 35 mL deionized water under vigorous magnetic stirring for 15 min. The obtained pink solution was transferred into a 50 mL Teflon-lined stainless-steel autoclave, and the cleaned Ni foam was immersed into the solution. The autoclave was sealed and maintained at 120 °C for 6 h. After being cooled to room temperature, the product on the Ni foam was carefully rinsed with deionized water and ethanol, and then dried at 60 °C for 12 h. The as-prepared precursors were transferred into a 50 ml Teflon-lined autoclave with 35 mL sodium sulfide solution (0.2 M) and kept at 120 °C for 14 h. Finally, the products were rinsed with deionized water and ethanol for several times, and then dried in a vacuum oven at 60 °C for 6 h.

2.2 Synthesis of $NiCo_2S_4$@CoS_x NTAs

An electrochemical workstation (Shiruisi, RST5200) was used to electrodeposit CoS_x nanosheets on the $NiCo_2S_4$ NTAs. The electrodeposition was performed on a three-electrode system by cyclic voltammetry (CV) at room temperature. A piece of Ni foam with $NiCo_2S_4$ NTAs was used as the working electrode, saturated calomel electrode (SCE) as the reference electrode, and a platinum plate as the counter electrode. 5 mM $Co(NO_3)_2{\cdot}6H_2O$ and 0.75 M thiourea were used as the electrolyte. The electrodeposition was carried out in the potential range from -0.6 to -1.2 V with a scan rate of 20 mV s^{-1} for 10 cycles. Then the products were carefully rinsed with deionized water and dried in a vacuum oven at 60 °C for 6 h.

2.3 Material characterization

The phase structures of the samples were identified by X-ray diffraction (XRD, Philips X'pert pro) with Cu Kα radiation (0.154056 nm). The morphologies of the obtained products were observed by a scanning electron microscope (SEM, Hitachi S-4800) and a high-resolution transmission electron microscope (HRTEM, FEI Tecnai G2 F30). The chemical composition was analysed by an in-situ energy dispersive X-ray spectrometer (EDX) equipped in the TEM. The mass changes of the samples were evaluated by a microbalance which has a readability of 0.01 mg (Mettler, XS105DU).

2.4 Electrochemical measurements

All the electrochemical measurements were also performed in 1 M KOH aqueous solution at room temperature with the electrochemical workstation. The $NiCo_2S_4$ NTAs (~2.5 mg) and the $NiCo_2S_4$@CoS_x NTAs (~2.78 mg) loaded Ni foam (10 mm × 10 mm × 1 mm) were used as the working electrodes. A platinum plate and a saturated calomel electrode were used as the counter and reference electrodes, respectively. The CV tests were carried out in the potential window of -0.15–0.55 V at scan rates ranging from 5 to 50 mV s^{-1} and the galvanostatic charge-discharge (GCD) tests were conducted in the potential window of 0–0.45 V at various current densities (5–50 mA cm^{-2}).

3 Results and discussion

The fabrication process of hierarchical $NiCo_2S_4$@CoS_x core/shell NTAs grown on Ni foam is schematically illustrated in Fig. 1. First, the $NiCo_2S_4$ NTAs were grown on three-dimensional Ni foam by a hydrothermal method followed by an anion exchange reaction in sodium sulfide solution. Second, the $NiCo_2S_4$ NTAs, serving as the backbones, were coated with the ultrathin CoS_x nanosheets after the electrodeposition, forming the unique hierarchical core/shell hybrid structures.

The X-ray diffraction (XRD) pattern of $NiCo_2S_4$ NTAs on Ni foam has been shown in Fig. S1†. The diffraction peaks at 26.7°, 31.6°, 38.3°, 50.5° and 55.3° correspond to the respective (220), (311), (400), (511) and (440) planes of the cubic type $NiCo_2S_4$ phase (JCPDS Card no. 20-0782). The EDX spectrum (Fig. S2†) indicates that the $NiCo_2S_4$ nanotubes are mainly composed of Ni, Co and S elements. However the low crystallinity and the limited amount of the CoS_x nanosheets, making it difficult for XRD to identity their existence. The chemical composition of the $NiCo_2S_4$ nanotubes and the CoS_x nanosheets was confirmed by EDX spectrum (Fig. S2†). It clearly reveals that the CoS_x nanosheets are mainly composed of Co and S, except the Cu and C signals from the carbon-supported copper grids. The Co/S atomic ratio is about 1.53, which indicates that the chemical composition of the CoS_x nanosheets is not pure CoS, but also likely contains $CoO/Co(OH)_2$ as previously reported.[37, 38]

Fig. 2a presents a low magnification SEM image of the $NiCo_2S_4$ nanostructures on Ni foam. It shows that numerous slim

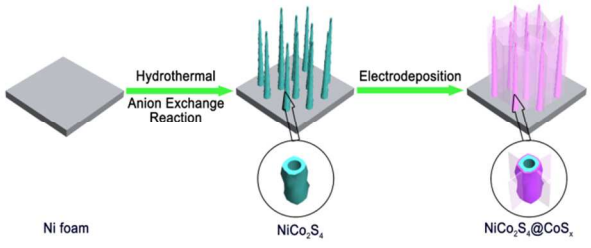

Fig. 1 Schematic illustration of the fabrication process of the $NiCo_2S_4$@CoS_x core/shell NTAs grown on Ni foam.

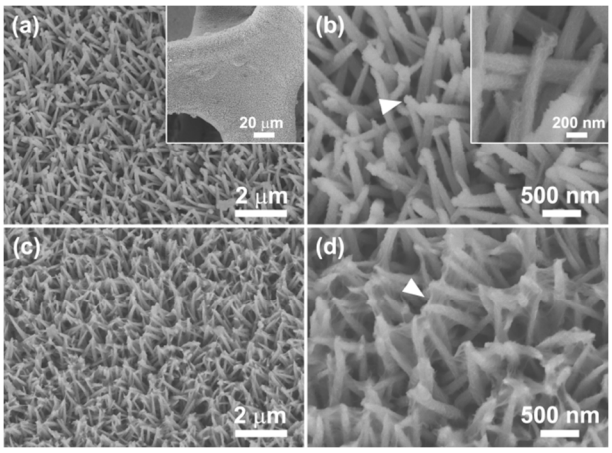

Fig. 2 SEM images of the $NiCo_2S_4$ NTAs (a and b) and $NiCo_2S_4$@CoS_x NTAs (c and d) grown on Ni foam at different magnifications.

nanowires are homogeneously aligned on the surface of the Ni foam on a large scale. The $NiCo_2S_4$ nanowires have a diameter of 60–100 nm, spaced apart adequately (the region marked by a white triangle), as shown in Fig. 2b. A higher magnification SEM image (Fig. 2b) further indicates that the $NiCo_2S_4$ nanowires have a rough surface, which is different from their precursors with a relatively smooth surface (Fig. S3†). It was due to the rapid rate of anion exchange reaction during the hydrothermal vulcanization process, as observed in previous reports.[23] After electrodeposition, the $NiCo_2S_4$ nanowires are uniformly decorated with ultrathin CoS_x nanosheets, forming hierarchical core/shell structures, as shown in Fig. 2c. A magnified SEM image (Fig. 2d) indicates that the ultrathin nanosheets with folded and silk-like morphology, in some regions (marked by a white triangle in Fig. 2d), band the $NiCo_2S_4$ nanowires together. Due to the three-dimensional porous structure of Ni foam (Fig. S4†) and the hierarchical core/shell structures of the active materials, the whole electrode with open and loose structures can have enough space and surface for the electrolyte ions diffusion during the fast reversible Faradaic reactions.

The morphologies and microstructures of the $NiCo_2S_4$ and the $NiCo_2S_4$@CoS_x were further investigated by TEM. Fig. 3a illustrates a typical TEM image of the $NiCo_2S_4$ nanostructures. It can be clearly seen that the $NiCo_2S_4$ nanowires are straight and hollow, indicating a tubular structure. It is probably related to the pseudo Kirkendall effect in the reactions of the $NiCo_2S_4$ precursors with S^{2-} ions in sodium sulfide solution. The outward diffusion of cobalt and nickel ions is faster than the inward diffusion of S^{2-} ions, thus the constant anion exchange reaction creates voids at the centre of the precursor nanowires and finally results in the $NiCo_2S_4$ nanotubes.[39, 40] It is found that the $NiCo_2S_4$ nanotube shows a very thin wall (~15 nm in thickness) and a slight rough surface, as shown in Fig. 3b. The diameters of the $NiCo_2S_4$ nanotubes range from 60 to 100 nm, with lengths of 2–4 μm from the tips to their roots contacting with Ni foam (inset of Fig. 3b), which is in good agreement with the observations from the SEM images. Fig. 3c presents a HRTEM image of the $NiCo_2S_4$ nanotube with a good crystallinity. The insert of Fig. 3c is a higher magnification of the region marked by a red square, which reveals that the *d*-spacing of 0.284 nm corresponds to the distance of the (400) plane of the cubic type $NiCo_2S_4$. Fig. 3d presents a low magnification of the $NiCo_2S_4$@CoS_x hybrid structures. It is evidently observed that the $NiCo_2S_4$ nanotubes were coated with ultrathin CoS_x nanosheets, and formed a hierarchical core/shell hybrid structure. From Fig. 3e and f, the nanosheets with a thickness of several nanometres, coated on the surface of the $NiCo_2S_4$ nanotubes and connecting some of them together, are structurally continuous. With the nanosheets stretching out, they present a low crystallinity. Many nanosized open pores were found in the nanosheets, which is consistent with previous observations.[19, 41] Compared with traditional electrode materials, such hierarchical core/shell hybrid structures can offer many advantages. The $NiCo_2S_4$ nanotubes have a high electrical conductivity and a tight physical contact with Ni foam, which

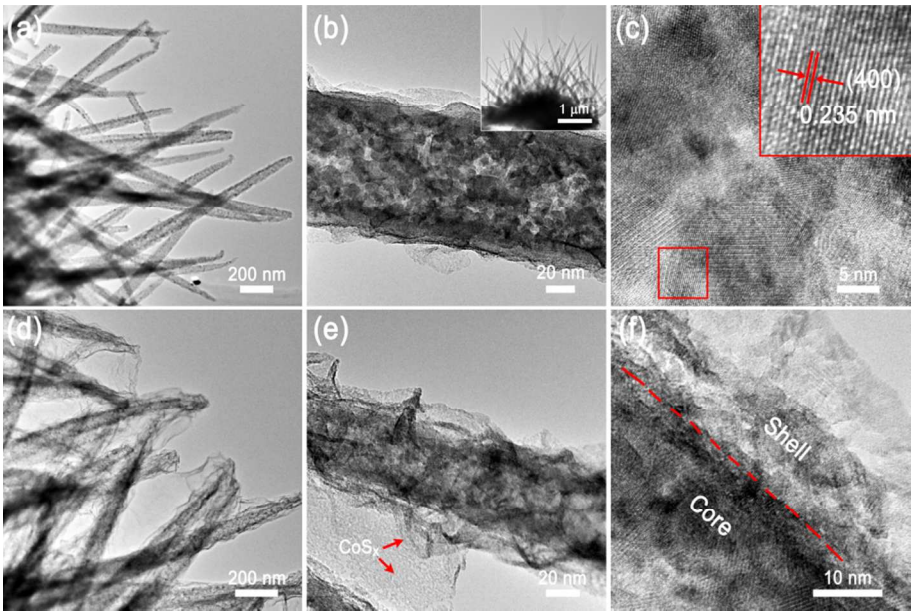

Fig.3 TEM images (a and b) and HRTEM image (c) of the $NiCo_2S_4$ NTAs. TEM images (d-f) of the $NiCo_2S_4$@CoS_x core/shell NTAs under different magnifications.

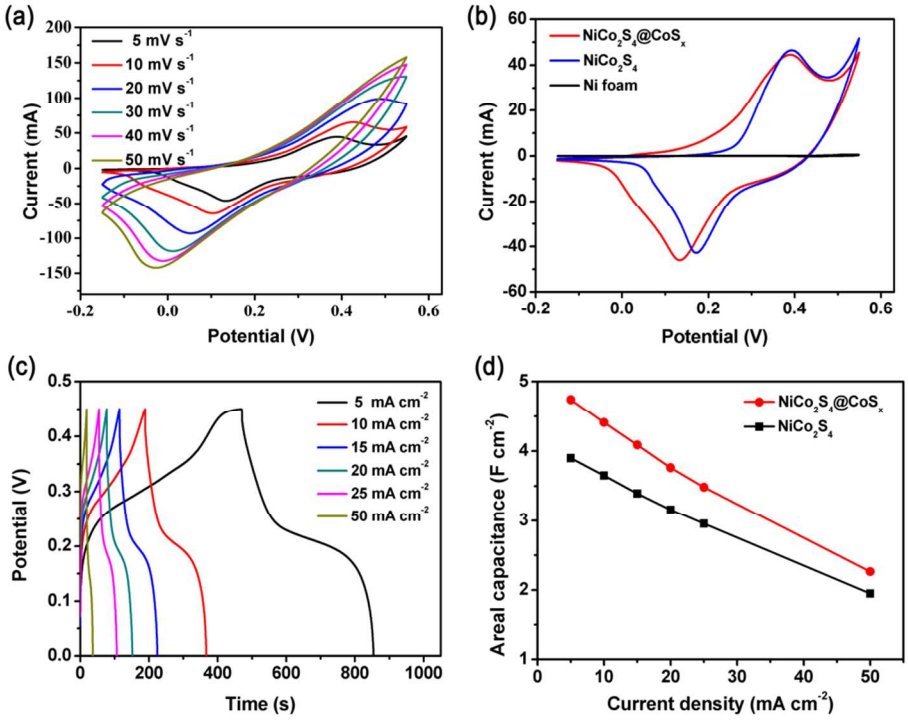

Fig. 4 (a) CV curves of the $NiCo_2S_4$@CoS_x electrode. (b) A comparison of CV curves of the $NiCo_2S_4$@CoS_x and $NiCo_2S_4$ electrodes at a same scan rate of 5 mV s^{-1}. (c) GCD curves of the $NiCo_2O_4$@CoS_x electrode at various current densities. (d) The areal capacitances of the $NiCo_2S_4$@CoS_x and $NiCo_2S_4$ electrodes at different current densities.

result in a stable and conductive structure for electron transport. The ultrathin CoS_x nanosheets, coated on the $NiCo_2S_4$ backbones, provide more surface area for the electrode materials to contact the electrolyte ions.

To evaluate the electrochemical performance, the $NiCo_2S_4$ NTAs and $NiCo_2S_4$@CoS_x NTAs were directly used as binder-free electrodes for supercapacitors. Fig. 5a shows the CV curves of the $NiCo_2S_4$@CoS_x electrode were achieved within a potential window of -0.15–0.55 V *vs* SCE at different scan rates ranging from 5 to 50 mV s^{-1}. The shape of the CV curves clearly indicates the existence of the Faradaic redox reactions and the distinct pseudocapacitive characteristics of the electrode materials. The redox reactions are mainly based on the reversible processes of Ni^{2+}/Ni^{3+}, Co^{2+}/Co^{3+} and Co^{3+}/Co^{4+} transitions.[15, 42] As the scan rates increase, the current density gradually increases. The anodic peaks shift to the anodic direction and the cathodic peaks shift to the cathodic direction, indicating that the fast reversible Faradaic reactions occur at the interfaces between the electroactive materials and the electrolyte. For comparison, the CV curves of the $NiCo_2S_4$@CoS_x, $NiCo_2S_4$ and Ni foam electrodes at the same scan rate of 5 mV s^{-1} are displayed in Fig. 4b. It is noteworthy that the CV curve of the Ni foam electrode comes closer to a straight line, suggesting that the contribution of the Ni foam to the capacitance can be neglected. Moreover, the integrated CV area of the $NiCo_2S_4$@CoS_x electrode is larger than that of the NCo_2S_4 electrode, indicating that the presence of CoS_x nanosheets in the $NiCo_2S_4$ NTAs significantly enhance the areal capacitance of the whole electrode.

GCD measurements were conducted in a potential range of 0–0.45 V at various current densities ranging from 5 to 50 mA cm^{-2}. The GCD curves of the $NiCo_2S_4$@CoS_x and $NiCo_2S_4$ electrodes are displayed in Fig. 4c and Fig. S5†, respectively. The area capacitance C_a (F cm^{-2}) can be calculated from the GCD curves by the equation, $C_a = I\Delta t/(S\Delta V)$, where I (A) is the discharging current, Δt (s) is the discharging time, S (cm^2) is the area of the electrode and ΔV (V) is the discharging potential range. The effect of different amounts of CoS_x on the capacitive performance was examined and the results are displayed in Fig. S6†. The $NiCo_2S_4$@CoS_x electrode with the CoS_x electrodeposition for 10 cycles exhibits the highest areal capacitance. As shown in Fig. 4d, the calculated areal capacitances of the $NiCo_2S_4$@CoS_x electrode with the CoS_x electrodeposition for 10 cycles are 4.74, 4.41, 4.09, 3.76, 3.48 and 2.26 F cm^{-2} at the current densities of 5, 10, 15, 20, 25 and 50 mA cm^{-2}, respectively. For comparison, the $NiCo_2S_4$ electrode shows lower capacitances (3.89, 3.65, 3.39, 3.16, 2.95 and 1.95 F cm^{-2}) at the same current densities. It can be clearly found that the $NiCo_2S_4$@CoS_x electrode exhibits a high areal capacitance of up to 4.74 F cm^{-2} at 5 mA cm^{-2}, which is much higher than the $NiCo_2S_4$ electrode as well as many previously reported areal capacitances of the electrodes with core/shell hybrid structures, such as $NiCo_2O_4$@MnO_2 nanowire arrays (2.24 F cm^{-2} at 2 mA cm^{-2}),[35] ZnO@Ni_3S_2 nanowire arrays (2.29 F cm^{-2} at 3 mA cm^{-2}),[17] Co_3O_4@$NiCo_2O_4$ nanowire arrays (2.04 F cm^{-2} at 5 mV s^{-1})[32] and $Co_xNi_{1-x}(OH)_2$/$NiCo_2S_4$ nanotube arrays (2.86 F cm^{-2} at 4 mA cm^{-2}).[25] Such high areal capacitances evidently demonstrate the advantages of the hierarchical core/shell hybrid structures.

In addition, the cycling stability was also evaluated by the repeated charging–discharging measurements at a constant current density of 50 mA cm^{-2} for 1500 cycles, as shown in Fig. 5. The areal capacitances of the two electrodes show a slightly decrease with increasing cycle number. After 1500 cycles, the $NiCo_2S_4$ electrode exhibits a low areal capacitance of 1.21 F cm^{-2} and only 62.5% initial capacitance is retained. By contrast, the

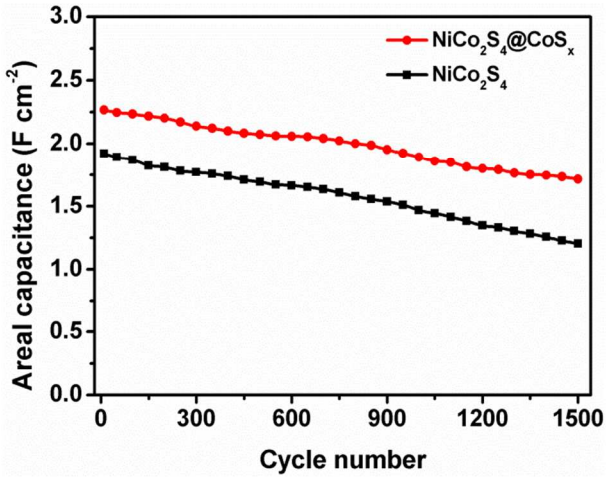

Fig. 5 Cycling performances of the $NiCo_2S_4$ and $NiCo_2S_4$@CoS_x electrodes at a current density of 50 mA cm^{-2} for 1500 cycles.

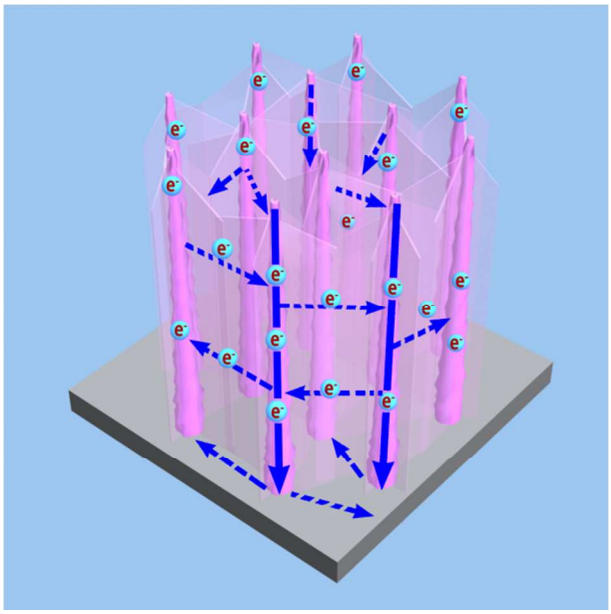

Fig. 6 Schematic illustration of electron transport pathway of the $NiCo_2S_4$@CoS_x NTAs on Ni foam.

$NiCo_2S_4$@CoS_x electrode maintains a relatively higher areal capacitance of 1.72 F cm^{-2} (~76.1% initial capacitance retention) after 1500 cycles. Such improved cycling performance of the hierarchical $NiCo_2S_4$@CoS_x NTAs can be attributed to the smart configuration. Furthermore, it is well noted that the cycling stability is evaluated at such high current density, which is meaningful and accords with the fast charge-discharge process for supercapacitors.[43]

Based on the superior pseudocapacitive performance of the $NiCo_2S_4$@CoS_x NTAs, the electron transport pathways are schematically proposed, as illustrated in Fig. 6. In our case, the smart configuration of the hierarchical $NiCo_2S_4$@CoS_x core/shell NTAs includes the following merits: First, the highly conductive Ni foam substrate can build up an express path for electron transport and the $NiCo_2S_4$ NTAs serve as the backbones which provide pathways for electrons. Generally, the highly ordered $NiCo_2S_4$ NTAs, contacting with Ni foam and forming a porous framework, will greatly benefit electron transport and electrolyte ions diffusion, which is the same as that in $NiCo_2S_4$ NTAs. Second, the CoS_x nanosheets were uniformly coated on the $NiCo_2S_4$ NTAs and connected the nanotubes together, providing more effective pathways for electrons than the individual $NiCo_2S_4$ NTAs. Third, the hierarchical $NiCo_2S_4$@CoS_x NTAs with open and loose structures have enough space and surface for the fast reversible Faradaic reactions. The ultrathin CoS_x nanosheets and the $NiCo_2S_4$ nanotubes with a thin tube wall (~15 nm) can make it easier for the electrolyte ions to diffuse into/out the nanotubes and the nanosheets. Thus, active materials can efficiently participate in the Faradic redox reactions and improve their utilization rate. In addition, this effective strategy of the hierarchical $NiCo_2S_4$@CoS_x core/shell NTAs can be expanded to other metal sulfides with core/shell hybrid structures for high-performance energy storage devices.

4 Conclusions

In summary, hierarchical $NiCo_2S_4$@CoS_x core/shell NTAs grown on Ni foam were successfully fabricated by an effective strategy. They were directly used as binder–free electrodes for supercapacitors and delivered a high areal capacitance, good rate capacity and cycling stability. Such superior capacitive performance achieved can be attributed to the smart configuration of the two electroactive materials. Compared with the $NiCo_2S_4$ NTAs, this smart configuration exhibits some considerable advantages, such as more electron transport pathways, better electrochemical stability and higher utilization rate of electrode materials. Therefore, the hierarchical $NiCo_2S_4$@CoS_x core/shell NTAs with superior electrochemical performance would have potential applications in supercapacitors. This work further demonstrates an effective strategy to design and fabricate metal sulfides with core/shell hybrid structures for energy storage devices.

Acknowledgements

This work was financially supported by the National Natural Science Foundation of China (Grant No. 61176058, 61404066 and 11474135) and the Scientific Research Foundation for the Returned Overseas Chinese Scholars.

Notes and references

School of Physical Science and Technology, Lanzhou University, Lanzhou 730000, China.
Fax: (+86) 931 8913554; Tel: (+86) 931 8912616;
Email: hanwh@lzu.edu.cn (Weihua Han); xieeq@lzu.edu.cn (Erqing Xie).

† Electronic Supplementary Information (ESI) available: [XRD pattern of the $NiCo_2S_4$ NTAs; EDX spectra of the $NiCo_2S_4$ nanotubes and the CoS_x nanosheets; SEM images of the $NiCo_2S_4$ precursors and cleaned Ni foam; GCD curves of the $NiCo_2S_4$ electrode]. See DOI:10.1039/b000000x/

1. A. S. Arico, P. Bruce, B. Scrosati, J.-M. Tarascon and W. van Schalkwijk, *Nat. Mater.*, 2005, **4**, 366.
2. J. R. Miller and P. Simon, *Science*, 2008, **321**, 651.
3. F. Beguin, V. Presser, A. Balducci and E. Frackowiak, *Adv. Mater.*, 2014, **26**, 2219.
4. K. Naoi, W. Naoi, S. Aoyagi, J.-i. Miyamoto and T. Kamino, *Acc. Chem. Res.*, 2012, **46**, 1075.
5. G. Wang, L. Zhang and J. Zhang, *Chem. Soc. Rev.*, 2012, **41**, 797.

6. L. Huang, D. Chen, Y. Ding, S. Feng, Z. L. Wang and M. Liu, *Nano Lett.*, 2013, **13**, 3135.
7. S. Liu, S. Sun and X. Z. You, *Nanoscale*, 2014, **6**, 2037.
8. D. T. Dam, X. Wang and J.-M. Lee, *Nano Energy*, 2013, **2**, 1303.
9. H. Chen, L. Hu, M. Chen, Y. Yan and L. Wu, *Adv. Funct. Mater.*, 2014, **24**, 934.
10. P. Yu, X. Zhang, D. Wang, L. Wang and Y. Ma, *Cryst. Growth Des.*, 2008, **9**, 528.
11. W.-j. Zhou, J. Zhang, T. Xue, D.-d. Zhao and H.-l. Li, *J. Mater. Chem.*, 2008, **18**, 905.
12. R. B. Rakhi, W. Chen, D. Cha and H. N. Alshareef, *Nano Lett.*, 2012, **12**, 2559.
13. K. M. Hercule, Q. Wei, A. M. Khan, Y. Zhao, X. Tian and L. Mai, *Nano Lett.*, 2013, **13**, 5685.
14. X. Lu, G. Wang, T. Zhai, M. Yu, J. Gan, Y. Tong and Y. Li, *Nano Lett.*, 2012, **12**, 1690.
15. H. Wan, X. Ji, J. Jiang, J. Yu, L. Miao, L. Zhang, S. Bie, H. Chen and Y. Ruan, *J. Power Sources*, 2013, **243**, 396.
16. S. Amaresh, K. Karthikeyan, I. C. Jang and Y. S. Lee, *J. Mater. Chem. A*, 2014, **2**, 11099.
17. Z. Xing, Q. Chu, X. Ren, C. Ge, A. H. Qusti, A. M. Asiri, A. O. Al-Youbi and X. Sun, *J. Power Sources*, 2014, **245**, 463.
18. T. Zhu, B. Xia, L. Zhou and X. Wen Lou, *J. Mater. Chem.*, 2012, **22**, 7851.
19. W. Chen, C. Xia and H. N. Alshareef, *ACS Nano*, 2014, **8**, 9531.
20. X. Rui, H. Tan and Q. Yan, *Nanoscale*, 2014, **6**, 9889.
21. Q. Wang, L. Jiao, H. Du, Y. Si, Y. Wang and H. Yuan, *J. Mater. Chem.*, 2012, **22**, 21387.
22. R. B. Rakhi, N. A. Alhebshi, D. H. Anjum and H. N. Alshareef, *J. Mater. Chem. A*, 2014, **2**, 16190.
23. H. Chen, J. Jiang, L. Zhang, D. Xia, Y. Zhao, D. Guo, T. Qi and H. Wan, *J. Power Sources*, 2014, **254**, 249.
24. H. Chen, J. Jiang, L. Zhang, H. Wan, T. Qi and D. Xia, *Nanoscale*, 2013, **5**, 8879.
25. J. Xiao, L. Wan, S. Yang, F. Xiao and S. Wang, *Nano Lett.*, 2014, **14**, 831.
26. J. Pu, T. Wang, H. Wang, Y. Tong, C. Lu, W. Kong and Z. Wang, *ChemPlusChem*, 2014, **79**, 577.
27. D. Cai, D. Wang, C. Wang, B. Liu, L. Wang, Y. Liu, Q. Li and T. Wang, *Electrochimica Acta*, 2015, **151**, 35.
28. C.-C. Hu, K.-H. Chang, M.-C. Lin and Y.-T. Wu, *Nano Lett.*, 2006, **6**, 2690.
29. Z. Lu, Q. Yang, W. Zhu, Z. Chang, J. Liu, X. Sun, D. Evans and X. Duan, *Nano Res.*, 2012, **5**, 369.
30. C. Guan, X. Xia, N. Meng, Z. Zeng, X. Cao, C. Soci, H. Zhang and H. J. Fan, *Energy Environ. Sci.*, 2012, **5**, 9085.
31. X. Xia, J. Tu, Y. Zhang, X. Wang, C. Gu, X.-b. Zhao and H. J. Fan, *ACS Nano*, 2012, **6**, 5531
32. G. Zhang, T. Wang, X. Yu, H. Zhang, H. Duan and B. Lu, *Nano Energy*, 2013, **2**, 586.
33. X. Liu, S. Shi, Q. Xiong, L. Li, Y. Zhang, H. Tang, C. Gu, X. Wang and J. Tu, *ACS Appl. Mater. Interfaces*, 2013, **5**, 8790.
34. W. Yang, Z. Gao, J. Ma, X. Zhang, J. Wang and J. Liu, *J. Mater. Chem. A*, 2014, **2**, 1448.
35. L. Yu, G. Zhang, C. Yuan and X. W. Lou, *Chem. Commun.*, 2013, **49**, 137.
36. H. X. Chuo, H. Gao, Q. Yang, N. Zhang, W. B. Bu and X. T. Zhang, *J. Mater. Chem. A*, 2014, **2**, 20462.
37. J.-Y. Lin, J.-H. Liao and S.-W. Chou, *Electrochimica Acta*, 2011, **56**, 8818.
38. Y. Sun, C. Liu, D. C. Grauer, J. Yano, J. R. Long, P. Yang and C. J. Chang, *J. Am. Chem. Soc.*, 2013, **135**, 17699.
39. J. Park, H. Zheng, Y.-w. Jun and A. P. Alivisatos, *J. Am. Chem. Soc.*, 2009, **131**, 13943.
40. X. Xia, C. Zhu, J. Luo, Z. Zeng, C. Guan, C. F. Ng, H. Zhang and H. J. Fan, *Small*, 2014, **10**, 766.
41. K. Xu, R. Zou, W. Li, Q. Liu, X. Liu, L. An and J. Hu, *J. Mater. Chem. A*, 2014, **2**, 10090.
42. L. Mei, T. Yang, C. Xu, M. Zhang, L. Chen, Q. Li and T. Wang, *Nano Energy*, 2014, **3**, 36.
43. P. Simon, Y. Gogotsi and B. Dunn, *Science*, 2014, **343**, 1210.

TOC

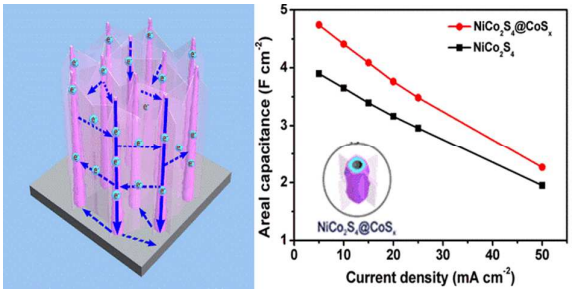

$NiCo_2S_4$@CoS_x core/shell nanotube arrays have been successfully synthesized and used to optimize the capacitive performance of electrochemical supercapacitors.